

The Sunyaev-Zeldovich Effect as Microwave Foreground and Probe of Cosmology

Gilbert P. Holder and John E. Carlstrom

*Department of Astronomy and Astrophysics, University of Chicago,
Chicago, IL 60637*

Abstract. The Sunyaev-Zel'dovich (SZ) effect from clusters of galaxies should yield a significant signal in cosmic microwave background (CMB) experiments at small angular scales ($\ell \gtrsim 1000$). Experiments with sufficient frequency coverage should be able to remove much of this signal in order to recover the primary anisotropy. The SZ signal is interesting in its own right; the amplitude and angular dependence are sensitive to both cosmology and the evolution of the gas. Combining CMB measurements with planned non-targeted SZ surveys could isolate the cosmological effects, providing CMB experiments with a low-redshift test of cosmology as a consistency check. Improvements in the determination of the angular diameter distance as a function of redshift from SZ and X-ray observations of a large sample of clusters will also provide a probe of cosmology.

1. Introduction

The Sunyaev-Zel'dovich (SZ) effect has been predicted for several decades (Sunyaev and Zel'dovich 1972), but it has only recently become a valuable observational tool. In the past few years, we have seen the observational programs go from ones aimed at detecting the effect to using it to map out massive clusters of galaxies (e.g., Birkinshaw 1999). In many ways, this is similar to the rapid evolution of CMB anisotropy experiments.

The SZ effect arises from hot gas between us and the surface of last scattering distorting the thermal spectrum of the CMB. This could describe a large variety of situations, but the SZ effect is usually discussed in the context of the effects of low redshift (below $z \sim 10$) gas that is heated mainly by gravitational infall in the course of structure formation. That will be the focus of this paper as well.

There are two SZ effects which are discussed. The first is the so-called thermal effect arising from Compton scattering, while the second is known as the kinetic effect, arising from simple Thomson scattering by a moving object.

The cool CMB photons traversing hot gas can undergo Compton scattering from the hot electrons, gaining a small amount of energy in the exchange. A typical fractional energy gain by the photons, in the non-relativistic limit of low electron and photon energies would be roughly $\frac{kT_{gas}}{m_e c^2}$ per collision. The cross-section for collision is simply the Thomson cross-section, σ_T , leading to an optical depth for a gas of electron number density n_e and characteristic size L of

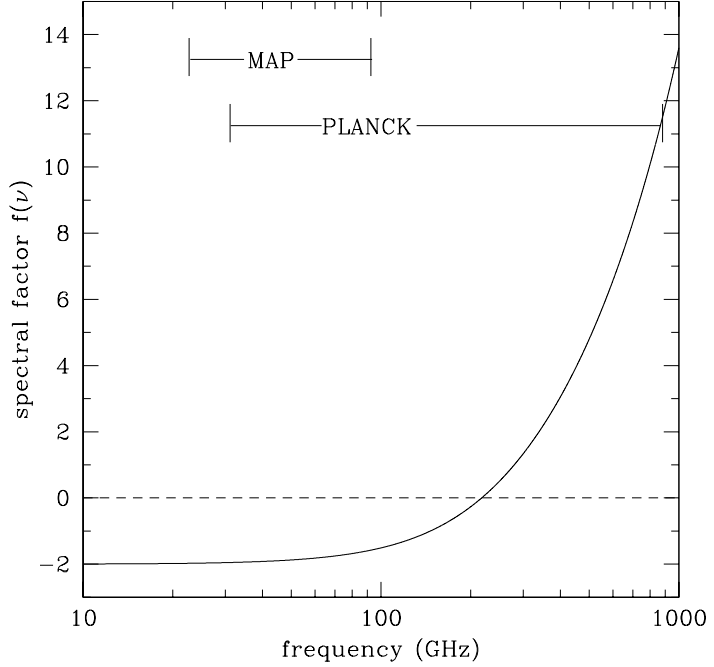


Figure 1. Spectral behavior of thermal SZ effect, where $\frac{\Delta T}{T_{CMB}} = f(\nu)y$, as a function of frequency, in the non-relativistic limit. Note that the high frequency area is far out in the Wien part of the CMB blackbody curve, and therefore there is very little signal to use to detect a temperature difference.

$\tau \sim n_e \sigma_T L$. Thus, the CMB photons as a whole should get a fractional energy gain roughly given by the Compton y parameter, defined as the fractional energy gain multiplied by the optical depth to scattering.

This scattering conserves photon number, so the net effect is to shift the CMB spectrum up in energy, distorting the blackbody curve slightly. This leads to a decrement at low frequencies, as more photons have been scattered out of those energy bins than have been scattered in, while there is an increment at high frequencies. The exact spectral form thus depends on the slope of the blackbody curve. The crossover frequency is near 217 GHz, with small relativistic corrections (Rephaeli 1995) making the crossover frequency a weak function of the gas temperature. This is a distinctly non-thermal spectrum, and CMB experiments with good frequency coverage will be able to easily distinguish this from purely thermal fluctuations. The spectral behavior is shown in Figure 1. In particular, note that the spectral behavior is slowly varying over the entire MAP CMB satellite experiment frequency coverage (22-90 GHz), and thus could be a difficult foreground to remove. On the other hand, the PLANCK satellite will have coverage from 30-850 GHz, allowing good sampling of the peculiar spectral behavior of the thermal SZ effect.

The kinetic effect arises from a moving mass of hot gas between us and the (mis-named in this case) surface of last scattering. The moving object sees a significant dipole in the CMB, with a hot spot in the direction of its motion. Thomson scattering will remove this dipole from the photons that undergo scattering. Back in the rest frame of the CMB, the gas will have created an apparent hot spot for observers that see the gas moving toward them and a cool spot for observers with the gas moving away from them.

The kinetic effect does not cause a deviation from a blackbody spectrum; it rather leads to a blackbody with a slightly different temperature. This means that the kinetic SZ effect has exactly the same spectral behavior as the primary CMB anisotropy. Thus, the kinetic effect is a foreground which is impossible to remove by spectral methods and it is important to understand its expected contributions to CMB anisotropy. Likewise, the primary CMB anisotropy can be a major source of confusion for determining peculiar velocities of clusters using the kinetic SZ effect.

The kinetic effect involves an energy shift per scattering which is effectively just a redshift, and thus on the order of (v_{bulk}/c) . Bulk peculiar velocities of clusters are expected to be less than $\sim 1000 \text{ km s}^{-1}$ in any cosmology. The thermal effect depends on the temperature of the electron gas, with an energy shift per scattering on the order of $\frac{kT_e}{mc^2}$. Assuming that the electrons and ions share the same temperature (Fox and Loeb 1997), the thermal energy in the gas is typically on the order $m_H v_\sigma^2$, where v_σ is the internal velocity dispersion in the potential well of the cluster, which can be $\sim 1000 \text{ km s}^{-1}$. At most frequencies, the thermal effect will be larger than the kinetic by a factor of ten or more.

The peculiar spectral behavior of the thermal effect means that the relative effects of the kinetic and thermal effects change with frequency, with the only SZ signal at the null of the thermal effect coming from the kinetic effect. It has been suggested that the peculiar velocity field of clusters could be mapped out in this way, but the small magnitude of the kinetic SZ effect makes this a very difficult experiment. Upper limits have been placed on the peculiar velocities of clusters (Holzapfel *et al.* 1997a), but a clear detection of the kinetic effect has not yet been observed.

2. Clusters of Galaxies

Clusters of galaxies are excellent sources of the SZ effect. Most of the baryonic mass of these objects is in the form of diffuse inter-galactic gas, heated to the virial temperature of the cluster. With cluster masses as large as $10^{15} M_\odot$ and radii of several Mpc, the gas can be $\sim 10 \text{ keV}$.

It is a fairly good approximation to take clusters as isothermal spheres with a truncation at the virial radius:

$$\rho(r) = \frac{\rho_\circ}{1 + (\frac{r}{r_c})^2} \quad \text{for } r < R_v \quad (1)$$

where the virial radius corresponds to the radius at which the infalling gas is shocked and converts much of its kinetic energy into thermal energy.

Assuming that the electron number density is also of this form, and that isothermality is a good approximation (Markevitch *et al.* 1998), then we can

derive a value for the central SZ effect:

$$\frac{\Delta T_o}{T_{CMB}} = 2 f(\nu) \frac{kT_{gas}}{m_e c^2} \sigma_T n_o r_c \arctan\left(\frac{R_\nu}{r_c}\right) \quad (2)$$

where $f(\nu)$ in the above gives the spectral dependence, approaching -2 in the Rayleigh-Jeans limit.

The SZ central decrement (at low frequencies) depends on the distribution of electrons in the cluster, with more condensed clusters having a stronger signal for a given mass. For a massive galaxy cluster, $n_o \sim 0.01 \text{ cm}^{-3}$, $T \sim 10 \text{ keV}$, $r_c \sim 250 \text{ kpc}$, and the virial radius is usually a factor of ten (or more) larger than the core radius. Using these numbers, we arrive at a central decrement of $\Delta T/T_{CMB} \sim 10^{-3}$. However, the central density and core radius are expected to vary from cluster to cluster in a poorly understood way, making the central decrement a difficult observable to understand.

The central decrement is a redshift-independent probe of clusters. The magnitude of the central decrement is sensitive to the degree of concentration of the cluster, as well as the path length along the line of sight through the cluster. For a given set of cluster properties, though, the central decrement does not depend on the redshift.

An observable that is much easier to understand is the total integrated SZ signal:

$$S \equiv S_o \int d\Omega \frac{\Delta T}{T_{CMB}} = S_o \int d\Omega \int dl f(\nu) \frac{kT_{gas}}{m_e c^2} \sigma_T n_e(l) \quad (3)$$

where S_o gives the conversion to physical units such as Jy. Writing the integral over solid angle as $dA = d\Omega D_A(z)^2$, with $D_A(z)$ the angular diameter distance, this becomes

$$S = S_o f(\nu) \frac{kT_{gas}}{m_e c^2} \sigma_T \frac{N_e}{D_A(z)^2} \quad (4)$$

with N_e the total number of electrons, which should be simply related to the total mass. Note that we have assumed nothing about the distribution of the mass, only that the gas is isothermal. Any experiment with a beam size larger than the cluster will not be sensitive to the degree of concentration of the gas. This is not the case for most observables of a system. For example, X-ray bremsstrahlung emission is proportional to $n_e^2 T^{0.5}$, making the integrated emission highly sensitive to the degree of concentration of the gas.

Finally, it is important to note that the SZ effect, as a distortion of the blackbody spectrum, is independent of redshift for a given set of cluster properties and therefore all redshifts contribute equally to the magnitude of the effect along a given line of sight. Of course, a nearby cluster will intersect more lines of sight, and thus will have a larger integrated effect over the sky, as seen by the inclusion of the angular diameter distance in the expression for the total integrated effect. Clusters are typically a few arcminutes in extent, so as long as the beam size is $\lesssim 1'$ the SZ effect is essentially independent of redshift. Even in the case of large beams, the redshift dependence is not particularly restrictive. For comparison, the angular diameter distance is smaller than the luminosity distance by a factor of $(1+z)^2$.

3. Observations

As for observations of intrinsic anisotropy in the CMB, observations of the SZ effect have progressed over the last several years from low S/N detections and upper limits to high confidence detections and detailed images. The dramatic increase in the quality of the observations is due to improvements both in low-noise detection systems and in observing techniques, usually using specialized instrumentation with which the systematics that often prevent one from obtaining the required sensitivity are carefully controlled. Such systematics include, for example, the spatial and temporal variations in the emission from the atmosphere and the surrounding ground.

The SZ effect observations so far have been targeted mainly toward X-ray luminous galaxy clusters. Large scale non-targeted surveys for the SZ effect could, in principle, provide a unique and powerful probe of the distant universe as discussed in section 5.1. The power of such surveys is due to the independence of the SZ effect on the redshift to the galaxy cluster or filament causing the scattering. Unfortunately, the sensitivity of the current instrumentation used to measure the effect is not high enough to allow a large region to be surveyed in a reasonable amount of time. This situation may change soon, as instruments with the required sensitivity are being planned now.

The existing observations of the SZ effect toward galaxy clusters can be roughly divided into two classes: 1) single dish observations toward low redshift galaxy clusters ($z < 0.2$) at resolutions of several arcminutes, and 2) interferometric observations of distant clusters ($z > 0.2$) at resolutions of roughly an arcminute and higher. A recent review of the observations can be found in Birkinshaw (1999). Here we discuss briefly a few of the results to provide the reader with a measure of the quality of the data presently available.

Motivation for obtaining measurements of the SZ effect toward galaxy clusters is provided by the ability to combine SZ effect and X-ray emission data to determine cluster distances, and therefore the Hubble constant, and also to determine the fraction of the total cluster mass contained in the hot gas. The distance measurements are compelling as the estimates do not share any of the systematics inherent in more traditional methods; the technique relies solely on an understanding of the cluster gas. The SZ effect distances do, of course, suffer from other systematics. The gas mass fraction determinations are compelling as the gas mass accounts for most of the known baryonic mass of the cluster (Forman and Jones 1982, White *et al.* 1993) and therefore the gas mass fraction allows a good measure of the baryonic mass fraction for the cluster. Furthermore, the baryonic gas mass fraction for massive clusters should reflect the universal value Ω_B/Ω_M . Thus, we can solve for Ω_M by using the cluster gas mass fraction and the value of Ω_B derived from big bang nucleosynthesis (BBN) calculations (Copi, Schramm, and Turner 1995) constrained to fit the observed primordial abundance of light elements (e.g., Burles and Tytler 1998).

As discussed in Birkinshaw (1999), the first measurements of the SZ effect were made with single dish radio telescopes. Successful detections were obtained, although the reported results show considerable scatter, reflecting the difficulty of the measurement (see earlier review by Birkinshaw 1991 and references therein). These observations illustrated the need for telescopes and receiver systems designed explicitly to minimize differential atmospheric emis-

sion and ground pickup. Recent state-of-the-art single dish observations at radio (Herbig *et al.* 1995, Myers *et al.* 1997) and at millimeter wavelengths (Wilbanks *et al.* 1994, Holzapfel *et al.* 1997b) have resulted in significant detections of the effect and limited mapping. Observations near the null of the thermal effect have been made in an attempt to measure the peculiar velocities of galaxy clusters. An upper limit of about 2000 km s^{-1} has been set for the $z \sim 0.2$ clusters Abell 2163 and Abell 1689 by Holzapfel *et al.* (1997a), who also report a significant detection of the increment at frequencies above the null (see also Lamarre *et al.* 1998).

Interferometric techniques have been used to produce high quality images of the SZ effect (e.g., Jones *et al.* 1993, Grainge *et al.* 1993, Carlstrom, Joy, and Grego 1996, Grainge *et al.* 1996, Carlstrom *et al.* 1998). The high stability of interferometry is being exploited to make these observations. Interferometry also provides data on the cluster over a large range of angular scales making it possible to remove contaminating emission from individual radio sources. Lastly, it is possible to produce two-dimensional images of the SZ effect with interferometry. We show in Figure 2 four of the 27 clusters imaged with the cm-wave SZ effect experiment on the OVRO¹ and BIMA² interferometers (Carlstrom *et al.* private comm.).

In his recent review of the SZ effect, Birkinshaw (1999) provides a summary of Hubble constant determinations from the above single dish and interferometric, as well as other, SZ effect observations of clusters with redshifts as high as 0.55. The mean value of the derived Hubble constants is $\sim 60 \text{ km s}^{-1} \text{Mpc}^{-1}$ with no meaningful constraint on the deceleration parameter. The scatter in the Hubble constant measurements is of order $20 \text{ km s}^{-1} \text{Mpc}^{-1}$. Birkinshaw points out, however, that many of the observational uncertainties, such as the X-ray and radio absolute flux scales are correlated between the observations.

Two groups have reported cluster gas fractions based on SZ effect data (Myers *et al.* 1997, Grego 1999, Grego *et al.* 1999). Myers *et al.* use their single dish SZ effect observations combined with β -models for the gas density distribution constrained by X-ray imaging data, and with gas temperatures determined by X-ray spectroscopy, to determine the gas mass fractions f_g for a sample of four clusters. They report $f_g h = 0.061 \pm 0.01$ for three nearby clusters, although a fourth cluster in their sample gives $f_g h = 0.166 \pm 0.014$. Grego *et al.* report the results for 18 clusters imaged with the OVRO and BIMA cm-wave interferometric SZ system. They use the SZ effect data itself to constrain the β -models and X-ray spectroscopy for the gas temperatures. For the entire sample spanning redshifts from 0.171 to 0.826 and assuming an open $\Omega = 0.3$ cosmology, they find $f_g h = 0.077^{+0.006}_{-0.010}$ scaled to r_{500} , the radius at which the overdensity of the cluster is 500. Using only clusters with redshifts less than 0.25 so that the cosmology assumed will have little effect on the gas mass fractions derived, they find $f_g h = 0.085^{+0.011}_{-0.145}$, again scaled to r_{500} .

¹An array of 10.4 m mm-wave telescopes located in the Owens Valley, CA and operated by Caltech.

²An array of ten 6.1 m mm-wave telescopes located at Hat Creek, California and operated by the Berkeley-Illinois-Maryland-Association

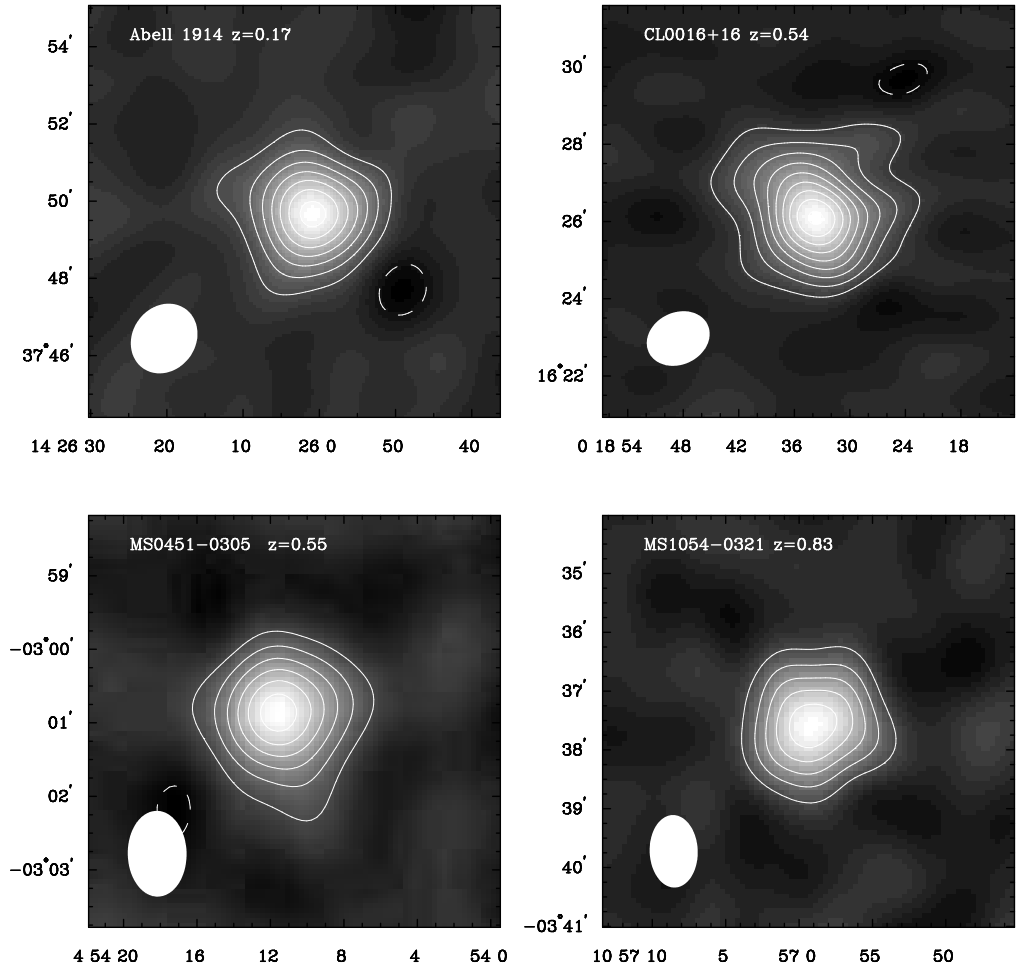


Figure 2. Images of the the SZ effect observed toward four galaxy clusters with similar luminosities, but spanning redshifts from 0.17 to 0.83. For all four clusters the contour levels are integer multiples of $-75 \mu K$, which corresponds to 1.5 to 5 times the noise level, depending on the cluster. The solid white ellipse in the bottom left corner of each panel represents the effective resolution of the image. The comparable SZ decrement observed for each cluster illustrates the independence on the SZ effect signal on redshift. The data were taken with low-noise cm-wave receivers installed on the OVRO and BIMA mm-wave interferometric arrays.

Assuming that the baryonic mass fraction for clusters equals the universal value and using $\Omega_B h^2 = 0.019 \pm 0.001$ determined from BBN and primordial abundance measurements (Burles and Tytler 1998), these gas mass fractions imply $\Omega_M h \sim 0.25$.

Future improvements in SZ effect observations, such as dedicated interferometric arrays and single dish telescopes equipped with bolometric arrays, will allow detailed imaging of many more than the order 30 clusters imaged to date and should allow definitive measurements of the Hubble constant and deceleration parameter. Commensurate improvements in the absolute calibration scale for both the radio and X-ray observations are also needed and will be provided, in part, by the AXAF/Chandra satellite at X-ray wavelengths, and by careful ground based efforts and by the planned CMB satellite missions at radio wavelengths. The expected increase in sensitivity and imaging speed will make large scale non-targeted surveys of the SZ effect possible, allowing a complete inventory of clusters at high redshifts.

4. The SZ Effect at Higher Redshifts

The imprint of distant clusters on the CMB has two important implications. As the SZ effect is the upscattering of CMB photons, it should come as no surprise that this can be a contaminant in CMB experiments. The thermal SZ effect can become larger than the CMB signal around $\ell \gtrsim 2000$, depending on the cosmology and cluster properties. The thermal effect has a distinctive frequency signature, allowing a multi-frequency experiment with sampling on both sides of the null (near 217 GHz) to separate it from intrinsic CMB anisotropy. The kinetic SZ effect cannot be spectrally distinguished from the primary CMB anisotropy, and could be impossible to remove from the data. Fortunately, the kinetic signal is expected to be much lower than the thermal signal, and thus never becomes dominant.

While Planck has frequency channels that trace out the thermal SZ spectrum on both sides of the null, this is not the case for MAP which only has frequency coverage up to 90 GHz. For the thermal SZ effect, this is still fairly far into the Rayleigh-Jeans region, where the signal becomes independent of frequency. Thus, there is very little leverage for inferring the amount of SZ contamination in measurements of the CMB. Several papers have investigated the expected anisotropy due to high-redshift clusters (Cole and Kaiser 1989, Atrio-Barandela and Muecket 1999, Colafrancesco *et al.* 1994). We discuss the contribution of the SZ effect to the angular power spectrum in section 5.2.

The second major implication is that surveys could be done to search for this effect to map out the cluster abundance as a function of redshift. This is expected to be a powerful probe of cosmology (e.g., Barbosa *et al.* 1996, Colafrancesco *et al.* 1997) as discussed in section 5.1.

However, both the level of CMB contamination and the evolution of the cluster abundance depend on cosmology and cluster physics. It is expected that the dependencies are different for the two observables, and combining CMB measurements with deep surveys should together separate cosmological evolution of the number density from evolution of the gas properties.

In this section, we will lay out the tools required to probe high-redshift clusters. Both the comoving number density and the physical properties of clusters are expected to evolve with redshift. The number density evolution of clusters of a given mass is fixed by the cosmology, while a model is needed to relate mass and temperature as a function of redshift. Beyond this, X-ray studies indicate that the distribution of gas within clusters also evolves with mass and redshift, and must also be taken into account. We will deal with these points, in turn, below.

4.1. Cosmological Evolution of Cluster Abundances

The prospect of using the SZ effect to detect high-redshift clusters is very exciting. Presumably, an SZ experiment should be able to find clusters at any redshift, given high sensitivity and large sky coverage. The expected number of clusters at a given sensitivity depends both on the cosmology and the history of the cluster gas.

In a low-density universe, structure stops forming when the expansion starts to be driven by either curvature or a cosmological constant. If we live in a low-density universe, the structure that we now see, by and large, also existed out to a redshift of $z \sim 1$ and should be detectable out to those redshifts. In a critical-density universe, the structure that we now see probably formed very recently, and thus would not be detectable at high redshift. This means that a given patch of sky should contain more clusters in a low-density universe. Since the SZ effect is redshift-independent, all of these clusters should be detectable.

To illustrate this, we will show results generated by assuming that the Press-Schechter (Press & Schechter 1976) formula for the evolution of the number density with redshift is correct. We will adopt two models with one having $\Omega_M = 1.0, \Omega_\Lambda = 0.0, h = 0.5, \sigma_8 = 0.6$ and the other having $\Omega_M = 0.3, \Omega_\Lambda = 0.7, h = 0.6, \sigma_8 = 1.0$. and the usual CDM shape parameter for the power spectrum was taken to be $\Gamma = 0.25$. Both of these models reproduce the local cluster abundance (Viana and Liddle 1999), within the rather large errors.

All work was done assuming a global baryon fraction $f_b = 0.2$. This is in reasonable agreement with observations of X-ray emissions (Evrard 1997, Mohr, Mathiesen, and Evrard 1999) and SZ decrements (Myers *et al.* 1997, Grego *et al.* 1999) from clusters. Comparison between expected yields from BBN (Copi, Schramm, and Turner 1995) and abundances of light elements requires that $\Omega_b h^2 = 0.02$ (Burles and Tytler 1998). While the assumed baryon fraction is consistent with BBN for $\Omega_M = 0.3$, this is not the case for $\Omega_M = 1$. Thus, our results may overpredict the expected SZ signal in high-density universes, if BBN is correct and the measured baryon fractions are in error.

The Press-Schechter formula gives the number density of virialized objects of a given mass, specifically excluding any mass which is not virialized. This would be missing SZ signal from structures which have been significantly heated but are not yet virialized. Thus, the results here are most likely to be underestimates of the total SZ signal from clusters, although the importance of this effect has yet to be convincingly demonstrated.

For all of the results shown here, a lower mass limit of $10^{12} M_\odot$ was chosen, since masses below this would probably have cooled on a timescale much shorter than a Hubble time. The reason for this is twofold. First of all, low-mass objects

are cooler to start with, and thus have less energy to radiate. Secondly, cooling becomes increasingly efficient per unit mass at lower temperatures.

4.2. Mass-Temperature Relation

Press-Schechter gives a prediction for the number densities of objects of various masses, while the SZ effect is sensitive to both the number of electrons along the line of sight and the gas temperature. A conversion between mass and SZ signal is therefore required.

The gas temperature can be obtained by assuming that the gas is in virial equilibrium. Virial equilibrium requires that $kT \propto \frac{GM_v}{R_v}$. The exact constant of proportionality depends on the distribution of mass inside the cluster.

We need an estimate of the virial radius to get a mass-temperature relation. This is usually done by assuming the spherical collapse model. A region that is overdense relative to the critical density will eventually pull out of Hubble flow, turn around and collapse. The time of turnaround will be at exactly half the time of eventual collapse. Assuming that the epoch of observation is the epoch of formation, the turnaround radius of an observed cluster can be easily calculated given a cosmology. Ignoring Λ , the virial relation asserts that $2K = -W$, where K and W are the total kinetic and gravitational potential energy, respectively. Given that $K = 0$ at turnaround and energy is conserved, this indicates that $W_v = 2W_{ta}$ (where ta subscripts indicate properties at turnaround). This directly leads to $R_v = \frac{R_{ta}}{2}$. Including the effects of Λ modify this relation slightly (Lahav *et al.* 1991).

At the same time, the background universe has been expanding, changing the relative overdensity of the bound region. The mean overdensity of the bound region thus depends on the cosmology. Fitting functions are given by Bryan and Norman (1998) for the mean overdensity relative to the critical density, with their fit for a universe with $\Omega_M + \Omega_\Lambda = 1$ given by

$$\Delta(z) = 18\pi^2 + 82x - 39x^2 \quad (5)$$

where $x = \Omega_M(z) - 1$.

The viral relation tells us that $kT_{gas} \propto GM/R_{vir}$, but the exact constant of proportionality depends on the distribution of matter. For this, we turn to numerical simulations. Using the normalization of Bryan and Norman (1998), and a notation where $H(z) \equiv 100h E(z)$, we use

$$T_{gas} = 1.4 \times 10^7 (h^2 \Delta(z) E(z)^2)^{\frac{1}{3}} \left(\frac{M}{10^{15} M_\odot} \right)^{\frac{2}{3}} \text{ K} \quad (6)$$

For a critical density universe, equation 6 becomes very simple, with the temperature for a given mass scaling simply as $(1+z)$. This is easy to understand, since all lengths (including the virial radius) will scale as $(1+z)^{-1}$, so $GM/R_v \propto (1+z)$.

4.3. Evolution of Cluster Gas

Evolution of cluster gas must also be taken into account. The sizes of clusters are expected to evolve with the redshift of formation, with higher temperatures,

and therefore a stronger SZ signal for a given mass at higher redshift. For the total SZ effect flux for a cluster, this gets diluted by the decreasing angular extent, but the central decrement suffers no such dilution. In fact, since the central decrement $\propto \rho r T_{\text{gas}}$, and $T_{\text{gas}} r \propto M$, the central decrement for a fixed mass would be expected to nearly scale with the average gas density.

If clusters evolve self-similarly, the central decrement (for $\Omega_M = 1$) evolves as

$$\Delta T_o \propto k T_{\text{gas}} n_o r_c \propto M(1+z)^3 \quad (\text{self-similar}) \quad (7)$$

since $kT \propto GM/R$ and $n_o \propto (1+z)^3$.

The gas doesn't have to evolve this way, and X-ray observations seem to indicate that it does not (Kaiser 1991, Mohr, Mathiesen, and Evrard 1999). For example, if reionization dumped a substantial amount of entropy into the gas, or if the gas gained a significant amount of entropy during infall, it is reasonable that the core may not be able to adiabatically contract to form a compact core, and the core could be more diffuse than self-similarity would predict. The outer regions should be largely unchanged, giving a relation for the core radius:

$$r_c^2 \propto \frac{\rho_{\text{crit}}(z)}{\rho_c} R_v^2 \quad (8)$$

The self-similar solution has $\rho_c \propto \rho_{\text{crit}}$, and $r_c \propto R_v$. The core properties in that case are independent of cluster mass. If there is instead a minimum core entropy, then a gas with polytropic index 5/3 will have $\rho_c \propto T^{3/2}$. The core properties now depend on cluster mass, with lower masses having less concentration. Under these conditions, we obtain a different relation for the central decrement:

$$\Delta T_o \propto M \rho_{\text{crit}}(z)^{0.5} T_{\text{gas}}^{3/4} \propto M^{3/2} (1+z)^{9/4} \quad (\text{constant entropy core}) \quad (9)$$

for a fixed mass and a flat matter-dominated cosmology.

This is significantly different, both in its mass dependence and its redshift evolution. Thus, we would expect both qualitative and quantitative differences in counts above a given central decrement in the two gas evolution scenarios.

This is shown in the left panel of Figure 3. In this figure, we compare counts of clusters above a central decrement for self-similar scaling with a core:virial radii ratio of 1:10 and a constant entropy core model normalized such that a 9 keV cluster has a central electron number density of $2.0 \times 10^{-3} \text{ cm}^{-3}$. Counts are shown per square degree for both a flat matter-dominated model and a model with a cosmological constant. All calculations are done assuming an observing frequency of 30 GHz.

The two models for evolution form an envelope for each cosmology, probably bracketing the real evolution the gas follows. It can be seen that the range is enormous, with gas evolution equally important to the cosmological evolution.

Compare this with the right panel of Figure 3, where we show the counts per square degree for the same models, except now for all clusters with $S > 0.5 \text{ mJy}$. Recall that it was earlier stated that the total flux is independent of the gas distribution, assuming a constant baryon fraction, and isothermality. The constant entropy core model does not have a constant baryon fraction, with low-mass clusters having a lower baryon fraction. This is easy to understand,

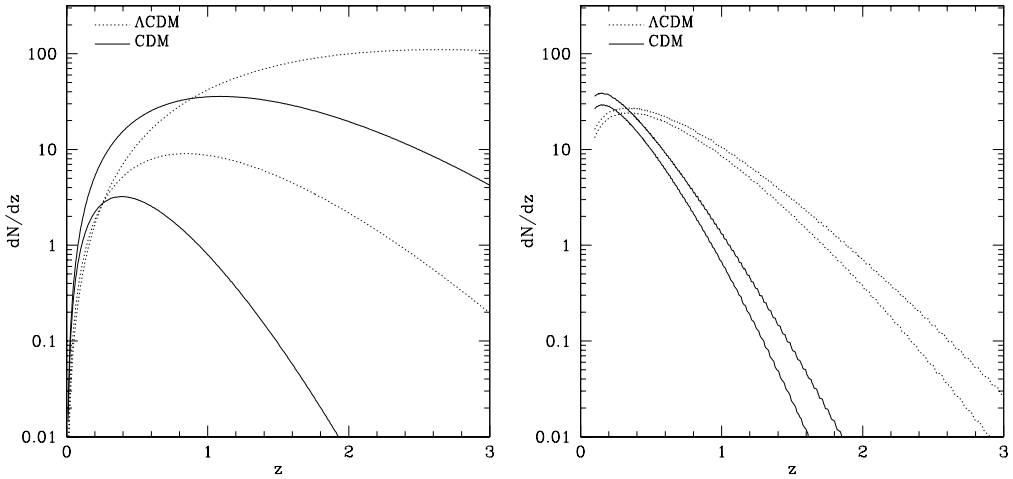


Figure 3. Counts per square degree of clusters with (left) central decrements above a threshold of $100\mu\text{K}$ (at 30 GHz) and (right) total flux density above 0.5 mJy . The upper curve (at high z) for each cosmology corresponds to self-similar evolution while the lower curve is for evolution with a constant entropy core.

as low-mass clusters have shallower potential wells, making it more difficult for pre-heated gas to fall in. Even for this case, it can be seen that the counts do not differ substantially from those expected from self-similar evolution, and cosmology is clearly the defining element.

5. Probing High-Redshift Clusters

Using the tools of the previous section, we can now estimate the expected signatures of high-redshift clusters. These can be studied in at least two ways: non-targeted SZ surveys and through the angular power spectrum of the anisotropy imprinted on the CMB. The next few years will see both of these methods implemented.

5.1. Non-Targeted SZ Surveys

Current observations of the SZ effect have been targeted at clusters which were known to have significant X-ray emission. Non-targeted surveys hold much promise for studying the evolution of the cluster abundance. Planned non-targeted SZ surveys are sensitive to both cosmology and gas evolution. Optical follow-up of SZ surveys will be conducted to obtain the redshift distribution. This redshift distribution is vital for finding the epoch of structure freeze-out, which is set by the redshift at which either curvature or Λ first becomes dynamically important. This redshift distribution allows an opportunity to differentiate between gas evolution and cosmological evolution of the abundance. This is shown in the left panel of Figure 3, showing the redshift distributions

of all clusters with a central decrement above a given value, for different gas evolution histories and cosmologies. Shown in the right panel of Figure 3 is the distribution of all clusters with a total flux density above a given threshold for two different cosmologies. The total flux density is almost independent of the gas evolution history, and is thus a very clean probe of cosmology.

Two things to note in Figure 3 are 1) the large number of expected clusters, and 2) the sensitivity of a small beam experiment to the gas evolution of clusters. The first point is interesting since the cluster mass threshold used for the plots have been selected to be within reach of planned SZ survey experiments. The importance of the second point will be shown in the next section where its effect on the angular power spectrum is discussed.

CMB experiments are expected to, in some ways, act as SZ cluster surveys. It is expected that satellite experiments should yield a large catalog of clusters. This will provide excellent information on the local abundance of clusters, but the catalog will not have much information on the redshift evolution. To underscore this point, we have compared expected cluster catalogs for full sky coverage with a high flux cut-off with a 12 deg² survey with much better sensitivity in Figure 4. This plot was done by assuming self-similar evolution, but it can be seen in Figure 3 that gas evolution does not have much of an effect on this sort of plot. The full-sky survey has a flux density cut-off of 20 mJy at 30 GHz, roughly comparable to the best expected performance of MAP or PLANCK. The high-sensitivity survey is given a flux density cut-off of 0.3 mJy, which may be possible with upcoming planned ground-based SZ surveys. While the large survey will yield more clusters, there is very little information beyond the local cluster abundance, which is already constrained by X-ray surveys (e.g., Viana and Liddle 1999). It is the evolution of the cluster abundance which is most important for cosmology.

5.2. Angular Power Spectrum

The power spectra of the thermal and kinetic effects are practically identical, with the main difference being an offset in amplitude by a factor of $\sim 10-20$. The power spectrum is easy to understand. At large angular scales (low ℓ), clusters are unresolved, acting like point sources. The angular Fourier transform of a point source has a flat amplitude, thus the c_ℓ spectrum is flat. At small angular scales (large ℓ), the clusters are resolved and the structure of the cluster is the important. If we take clusters to have $\rho \propto 1/(r_c^2 + r^2)$, then the angular SZ profile has $\Delta T \propto 1/\sqrt{\theta_c^2 + \theta^2}$. The angular Fourier transform of this is proportional to $\exp(-\theta_c \ell)/\ell$, giving $\ell^2 c_\ell \propto \exp(-2\theta_c \ell)$. Thus, a plot of $\ell(\ell + 1)c_\ell$ for a single cluster would rise as ℓ^2 at large angular scales, while it is suppressed as an exponential at small scales. The transition between these two regimes happens around the characteristic scale of a cluster, the core radius, leading to a peak in the power spectrum near $\ell \sim 2000$.

Both the amplitude and position of the peak of the angular power spectrum are sensitive to the chosen cosmology and the evolution of cluster gas. The amplitude at low ℓ is set by the total abundance of SZ effect-inducing clusters. The local abundance is fairly well constrained from X-ray observations, but the evolution with redshift is sensitive to cosmology. Since the SZ effect is redshift-independent, high-redshift clusters will contribute to CMB anisotropy as far

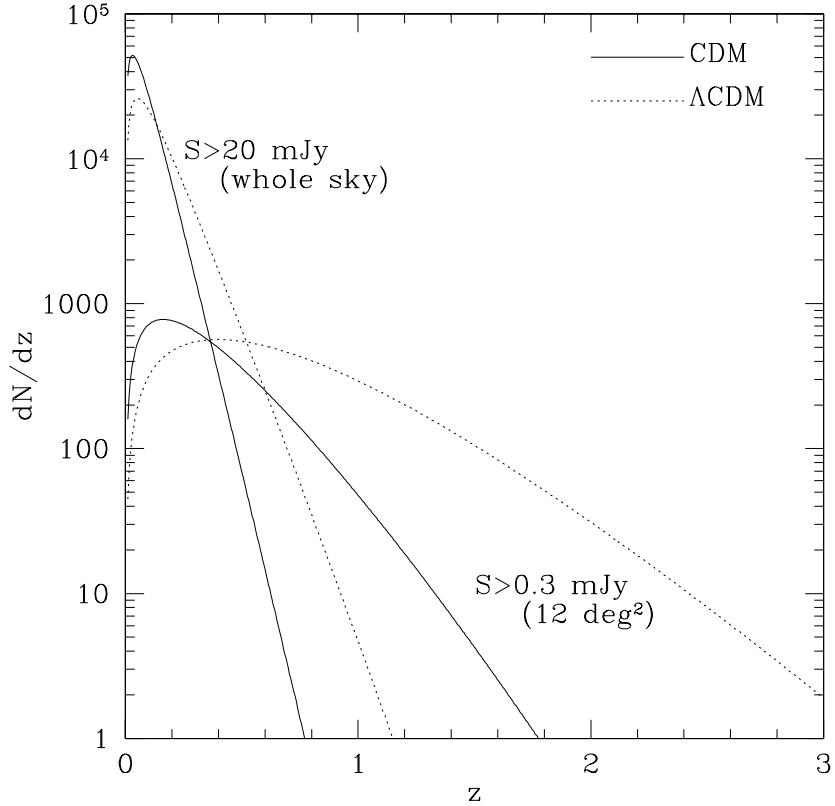


Figure 4. Expected number counts for two cosmologies for a low-sensitivity full-sky SZ survey such as PLANCK compared with possible upcoming ground-based surveys as a function of redshift.

back as they exist. This is particularly noticeable in the slope of the power spectrum at low ℓ 's. A model with a cosmological constant has a significant contribution from compact high-redshift sources, which have angular Fourier transforms which remain constant out to higher values of ℓ . Thus, the ΛCDM model stays close to a line going as ℓ^2 longer than the flat matter-dominated model.

The ratio of high- ℓ to low- ℓ contributions is effectively a measure of a weighted average of angular core radii. Self-similar evolution leads to much smaller cores for higher redshift clusters, and thus these power spectra have significantly more signal at high ℓ than their isentropic counterparts. Low-density universes have many more distant clusters (and thus more small-cored clusters) than high density universes, giving more power at high ℓ . These two mechanisms, gas evolution and cosmological evolution of the cluster abundance, can both change the average angular core radius and lead to comparable effects in the SZ power spectrum, making a clean interpretation of an SZ power spectrum difficult.

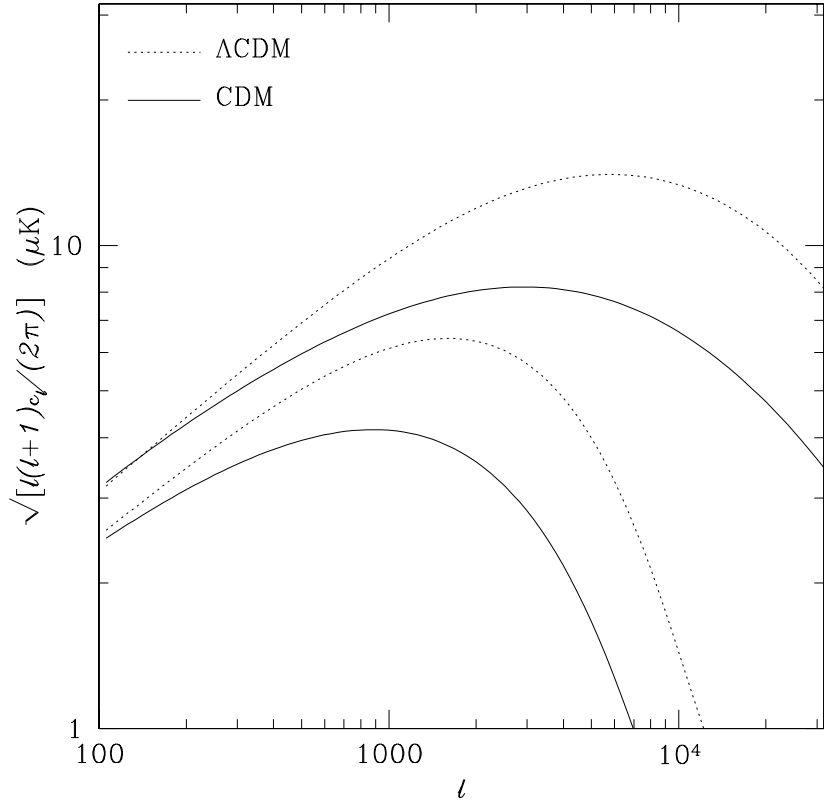


Figure 5. Angular power spectra $[\frac{\ell(\ell+1)c_\ell}{2\pi}]^{\frac{1}{2}}$ for two cosmologies and the two gas evolution histories. The top curve for each cosmology corresponds to self-similar evolution while the lower curve is for evolution with a constant entropy core

Shown in Figure 6 is the effect of removing all bright SZ sources above 20 mJy (at 30 GHz). While this is very effective at low ℓ , beating down the SZ signal by nearly a factor of 4, at high ℓ this has little effect. A large fraction of the signal at low ℓ 's comes from these clusters. The bulk of the high ℓ signal still comes from distant clusters, undetected individually. This is problematic, since it is exactly in this region where the SZ power spectrum starts to dominate over the signal from the primary anisotropy.

The thermal SZ effect does not approach the magnitude of the expected CMB anisotropy until $\ell \gtrsim 2000$. MAP has very little sensitivity at this scale, and most current CMB experiments are not sensitive at this scale either. However, many interferometric experiments have sensitivity at this scale, and upcoming experiments such as PLANCK should definitely pick up this SZ signal.

Added to this is uncertainty in the baryon fraction. Converting to BBN values would depress the expected power from SZ clusters in a flat matter-dominated universe by a factor of $0.2/\Omega_b$. While the evidence for BBN is strong,

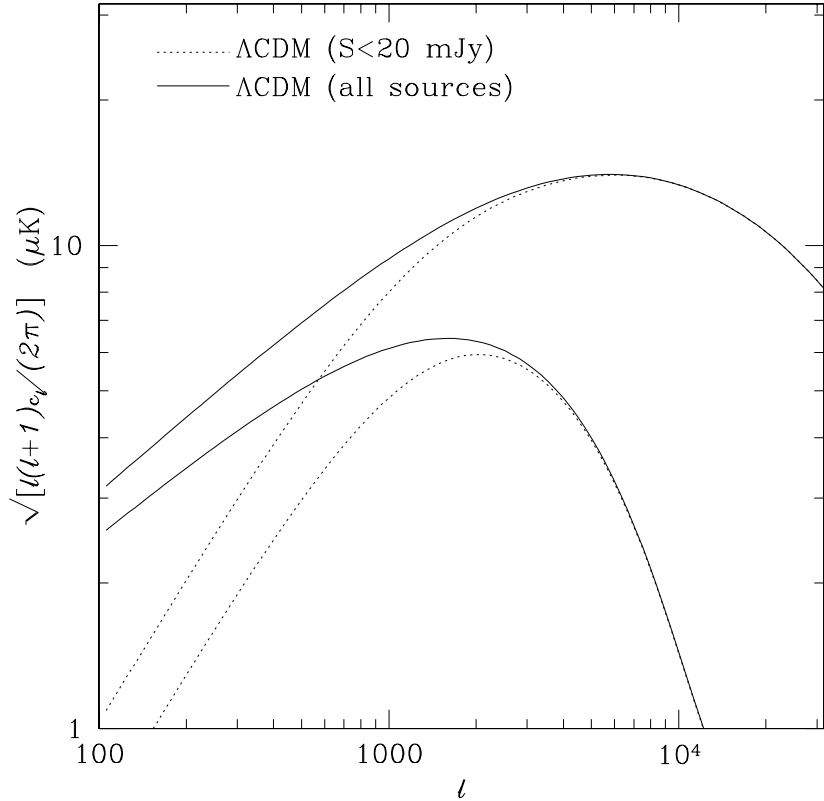


Figure 6. Angular power spectra $[\frac{\ell(\ell+1)c_\ell}{2\pi}]^{\frac{1}{2}}$ for a ΛCDM cosmology and the two gas evolution histories, showing the effect of removing all sources with a flux density greater than 20 mJy (at 30 GHz). The top curve (at high ℓ) for each cosmology corresponds to self-similar evolution while the lower curve is for evolution with a constant entropy core

the measured baryon fractions in clusters seem difficult to dismiss, making the choice of baryon fraction an important, but difficult one in the case of $\Omega_M = 1$.

6. Summary

The contribution to the CMB angular power spectrum by the SZ effect from galaxy clusters is discussed. At low ℓ the primary CMB anisotropy dominates the power spectrum. The SZ contribution rises roughly as ℓ^2 until $\ell \sim 2000$, where individual clusters are resolved. At these ℓ 's, the SZ contribution dominates that of the primary CMB anisotropy. Since the spectral distortion of the CMB induced by the SZ effect is distinctly non-thermal, it can be separated from intrinsic anisotropy for CMB observations which have broad frequency coverage.

A measurement of the contribution to the CMB anisotropy power spectrum from the SZ effect would provide a measure of the underlying cosmology, independent of the values derived from the primary anisotropy. Combining large-scale non-targeted SZ effect surveys currently under consideration and the SZ signal detected by CMB experiments should give an independent determination of Ω_m , Ω_Λ , and σ_8 .

In order to complement CMB experiments, it would be useful to have SZ effect surveys which can at least partially resolve clusters. As seen in Figures 3-6, it is important to have this structural information in order to constrain the evolution of the cluster gas. Since typical core radii will be $1'$ or less, it would be preferable to have a survey with a beam of this size or smaller.

The SZ effect should be more constructively considered as a low-redshift source of secondary fluctuations in the CMB rather than simply as a foreground, since the signature can be used as a direct constraint on cosmology.

References

Atrio-Barandela, F. and Muecket, J. 1999, ApJ, **in press**, astro-ph/9811158.

Barbosa, D., Bartlett, J., Blanchard, A., and Oukbir, J. 1996, A&A, **314**, 13.

Birkinshaw, M. 1991, *Physical Cosmology*, ed. J. Tran Thanh Yan, Editions Frontiers, page 177.

Birkinshaw, M. 1999, Physics Reports, **310**, 97.

Bryan, G. and Norman, M. 1998, ApJ, **495**, 80.

Burles, S. and Tytler, D. 1998, ApJ, **507**, 732.

Carlstrom, J. E., Grego, L., Holzapfel, W. L., and Joy, M. 1998, *Eighteenth Texas Symposium on Relativistic Astrophysics and Cosmology*, ed A. Olinto, J. Frieman, and D. Schramm, World Scientific, page 261.

Carlstrom, J. E., Joy, M., and Grego, L. E. 1996, ApJ, **456**, L75.

Colafrancesco, S., Mazzotta, P., Rephaeli, Y., and Vittorio, N. 1994, ApJ, **433**, 454.

Colafrancesco, S., Mazzotta, P., Rephaeli, Y., and Vittorio, N. 1997, ApJ, **479**, 1.

Cole, S. and Kaiser, N. 1989, MNRAS, **237**, 1127.

Copi, C., Schramm, D., and Turner, M. 1995, Science, **267**, 192.

Evrard, A. 1997, MNRAS, **292**, 289.

Forman, W. and Jones, C. 1982, ARA&A, **20**, 547.

Fox, D. and Loeb, A. 1997, ApJ, **491**, 459.

Grainge, K., Jones, M., Pooley, G., Saunders, R., Baker, J., Haynes, T., and Edge, A. 1996, MNRAS, **278**, L17.

Grainge, K., Jones, M., Pooley, G., Saunders, R., and Edge, A. 1993, MNRAS, **265**, L57.

Grego, L. 1999. *Galaxy Cluster Gas Fractions from Interferometric Measurements of the Sunyaev-Zel'dovich Effect*. PhD thesis, Caltech.

Grego, L., Carlstrom, J. E., Joy, M. K., Reese, E. D., Holder, G. P., Patel, S., Cooray, A. R., and Holzapfel, W. L. 1999, *ApJ*, **submitted**.

Herbig, T., Lawrence, C. R., Readhead, A. C. S., and Gulkis, S. 1995, *ApJ*, **449**, L5.

Holzapfel, W. L., Ade, P. A. R., Church, S. E., Mauskopf, P. D., Rephaeli, Y., Wilbanks, T. M., and Lange, A. E. 1997a, *ApJ*, **481**, 35.

Holzapfel, W. L. *et al.* 1997b, *ApJ*, **480**, 449.

Jones, M. *et al.* 1993, *Nature*, **365**, 320.

Kaiser, N. 1991, *ApJ*, **383**, 104.

Lahav, O., Rees, M. J., Lilje, P. B., and Primack, J. R. 1991, *MNRAS*, **251**, 128.

Lamarre, J. M. *et al.* 1998, *ApJ*, **507**, L5.

Markevitch, M., Forman, W. R., Sarazin, C. L., and Vikhlinin, A. 1998, *ApJ*, **503**, 77.

Mohr, J., Mathiesen, B., and Evrard, A. 1999, *ApJ*, **in press**, astro-ph/9901281.

Myers, S. T., Baker, J. E., Readhead, S., A. C., Leitch, E. M., and Herbig, T. 1997, *ApJ*, **485**, 1.

Rephaeli, Y. 1995, *ARA&A*, **33**, 541.

Sunyaev, R. and Zel'dovich, Y. 1972, *Comments Astrophys. Space Phys.*, **4**, 173.

Viana, P. and Liddle, A. 1999, *MNRAS*, **303**, 535.

White, S., Navarro, J., Evrard, A., and Frenk, C. 1993, *Nature*, **366**, 429.

Wilbanks, T. M., Ade, P. A. R., Fischer, M. L., Holzapfel, W. L., and Lange, A. E. 1994, *ApJ*, **427**, L75.